Damage in sheet metal forming: prediction of necking phenomenon

Nathalie Boudeau — Arnaud Lejeune — Jean-Claude Gelin

Laboratoire de Mécanique Appliquée R. Chaléat (LMARC)
UMR CNRS 6604
Université de Franche-Comté/CNRS
24 Rue de l'Epitaphe
F-25000 Besançon
nathalie.boudeau@univ-fcomte.fr

ABSTRACT. *Necking is a phenomenon limiting sheet metal-forming processes. The linearised perturbation technique is presented and adapted to various cases of yield criteria, damage models and 2D/3D stress states. Some aspects about calculations are given. Finally two applications of these works are shown. The first one validates the theory by establishing Forming Limit Diagrams. The second one is the implementation in a FE code and presents the necking predictions obtained on industrial cases of metal-forming.*

RÉSUMÉ. *La striction est un phénomène qui limite les opérations d'emboutissage. La technique des perturbations linéarisées est présentée et adaptée à des cas très variés de critères de plasticité, de modèles d'endommagement et d'états de contraintes 2D/3D. Quelques aspects calculatoires sont donnés. Enfin deux applications de ces travaux sont présentées. La première application valide la théorie par construction de Courbes Limites de Formage. La seconde est l'implémentation dans un code éléments finis et présente les prédictions de striction localisée obtenues dans des cas industriels d'emboutissage.*

KEYWORDS: *plastic instability, yield locus, damage model, prediction, FE simulation.*

MOTS-CLÉS : *instabilité plastique, surface de plasticité, modèle d'endommagement, prédiction, simulation EF.*

REEF – 10/2001. NUMEDAM'00, pages 295 to 310

1. Introduction

Necking in sheet metal forming arises quite naturally due to loading conditions, boundary conditions or material inhomogeneities that develop when plastic straining increases. In that field the pioneer works have been done in the early stage of the development of mathematical plasticity [HIL 52]. Lots of experimental works have been made to characterize the forming ability of the sheet with the introduction of the Forming Limit Diagrams (FLD) [KEE 65] [GOO 68]. Unfortunately, these curves are not intrinsic and depend strongly on the strain path that can be very complex in industrial forming processes, especially in case of multi-stage forming processes. Arrieux introduced then the Stress Limit Curves (SLC) [ARR 89]. These curves seems not to dependent on the strain path.

Concurrently, theoretical works were developed and numerous models were proposed. These models can be divided into two classes: models based on homogeneous continuum and models based on heterogeneous continuum.

The development of numerical methods to simulate the forming processes creates the necessity to predict necking phenomenon from FE results. The commercial codes as Pamstamp® and Optris® propose to plot the principal strain state calculated during the FE simulation on the experimental or calculated FLD without taking into account the fact that the necking state depends strongly upon the strain path. The early works done in the proposition of a criterion independent from the strain path and able to predict necking from FE results are due to two of the authors in [BOU 94]. Since these works several approaches have been proposed ([BRU 95], [BRU 97], [HOR 96], [KNO 00], [FRO 98]).

After this short introduction, the paper will continue with the second section devoted to the presentation of the linear perturbation and the numerous possibilities of this approach. Finally section 3 will present the results obtained in two cases: FLD computations and necking prediction during FE simulations.

2. The perturbation technique: theory and applications

2.1. *Theory*

Necking phenomenon is considered as an instability of the local equilibrium. To study this instability, the perturbations technique and its first order Taylor's development are employed [MOL 85]. Because necking occurs only in regions where plastic strains are quite important the local problem is strongly non-linear. Moreover the hypothesis of a rigid-plastic material is done.

The local equilibrium is defined by:

– the plastic yield locus,

– the hardening law,

– the constitutive law,
– the local equilibrium relationship,
– the compatibility of the deformation,
– the plastic incompressibility.

The hardening law is the Hollomon one with strain rate dependence:

$$\sigma_0(\bar{\varepsilon},\dot{\bar{\varepsilon}}) = K(\varepsilon_0 + \bar{\varepsilon})^{N_0}(\dot{\bar{\varepsilon}})^{M_0} \quad [1]$$

but other hardening laws can be used.

ε_0 is defined as $\sigma_Y = \sigma_0(0,\dot{\bar{\varepsilon}})$ with σ_Y the initial yield stress.

The local equilibrium conditions are the following:

$$(l\sigma_{ij})_{,i} = 0 \quad [2]$$

Where l corresponds to the wideness of the necking band (Figure 1).
The strain rate compatibility conditions and the plastic incompressibility are:

$$D_{ij,kl} + D_{kl,ij} = D_{ik,jl} + D_{jl,ik} \quad [3]$$

$$trace\underline{D} = D_{ii} = 0 \quad [4]$$

The local equilibrium can take the following form:

$$\mathsf{A}(U) = 0 \quad [5]$$

where A is a non linear operator and U a vector.
Vector U describes the strain and stress state for the mechanical equilibrium:

$$U = \left\{\sigma_{11}, \sigma_{22}, \sigma_{12}, \bar{\sigma}, D_{11}, D_{22}, D_{12}, D_{33}, \dot{\bar{\varepsilon}}\right\}^T \quad [6]$$

A perturbation vector δU is introduced to provide a way to detect plastic instability:

$$\delta U = \delta U^0 \exp(\eta t) \exp(i \xi x.n) \quad [7]$$

where δU^0 is the amplitude of the perturbation, ξ is the spatial part of the perturbation and η the temporal part of the perturbation. x and n are vectors that correspond respectively to the spatial location where necking could occur and to the normal vector associated with the necking band which could develop at the material point corresponding to the endpoint of the n vector as shown in Figure 1.

Thus if U^0 is the solution of [5] the perturbed vector:

$$U = U^0 + \delta U \qquad [8]$$

has also to satisfy equation [5]. In the small perturbations case, the Taylor's development to the first order gives:

$$\mathbf{A}\,(U^0, \varphi, \theta, \eta).\delta U^0 = 0 \qquad [9]$$

A non trivial solution for δU^0 is needed meaning that:

$$\det \mathbf{A}\,(U^0, \varphi, \theta, \eta) = P_{\varphi,\theta,U^0}(\eta) = 0 \qquad [10]$$

where $P_{\varphi,\theta,U^0}(\eta)$ is a polynomial of η.

Finally instability or necking occurs when:

$$\mathrm{Re}\,(\eta) > 0 \qquad [11]$$

Generally, the condition [11] is too severe and a positive value for the threshold ξ is used. So the necking criterion becomes:

$$\mathrm{Re}\,(\eta) > \xi \qquad [12]$$

The expression of equations [2] and [3] are different for 2D- or 3D-stress states. For 3D stress state under consideration, the stress tensor and the strain rate tensors are:

$$\underline{\sigma} = \begin{bmatrix} \sigma_{11} & \sigma_{12} & 0 \\ \sigma_{12} & \sigma_{22} & 0 \\ 0 & 0 & \sigma_{33} \end{bmatrix} \qquad \underline{D} = \begin{bmatrix} D_{11} & D_{12} & 0 \\ D_{12} & D_{22} & 0 \\ 0 & 0 & D_{33} \end{bmatrix} \qquad [13]$$

Equation [4] remains the same as in 2D case.

The vector position and normal vector to the localised band are given in Figure 1:

$$x = (x_1, x_2, x_3) \qquad n = (\sin\varphi.\cos\theta, \sin\varphi.\sin\theta, \cos\varphi) \qquad [14]$$

The local equilibrium is governed by equation [2] with:

$$l = \frac{h}{\sin\varphi} \qquad [15]$$

where l corresponds to the thickness of the necking band as shown in Figure 1.

The case $\varphi = 0$ is ignored because it corresponds to the case where the band is parallel to the sheet plane.

The perturbation of equation [2] taking into account equation [15] followed by a first order series expansion is given in appendix 1.

In case of 3D-stress state, there are six equations of compatibility. Only three equations are linearly independent. These three independent equations have been determined with the formal computation software Mathematica®. The perturbation followed by a Taylor's development of these equations is also given in appendix 1.

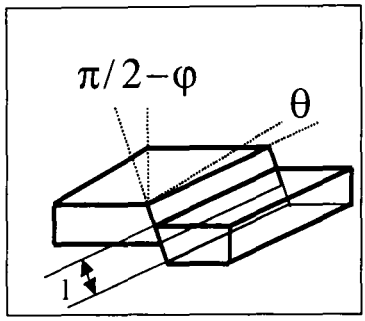

Figure 1. *Orientation of the necking band compared to the position vector in the reference frame. Model for necking in the case of 3D-stress state*

2.2. *Applications*

The aim of this section is to demonstrate the high flexibility of the linearized perturbations technique. The application of the method to several plastic yield loci and to damaged material is presented. The numerical results will be presented in the following paragraphs.

2.2.1. *Plastic yield locus*

There is a large variety of plastic yield loci that can be used to represent the sheet metal behaviour during stamping or deep drawing. They have been developed to give a better representation of the material flow in the case of large plastic deformation. The first anisotropic model is due to Hill [HIL 48] who proposed a quadratic model suitable for the behaviour of standard steel. It allows to model isotropic, transverse isotropic and orthotropic material that is well dedicated to describe the behaviour in sheet metal forming. The use of aluminium alloys in sheet metal-forming to decrease the weight of automotive parts revealed a lack of the Hill 48 criterion to describe the so called anomaly of aluminium and several others criteria were developed ([BAS 77], [BAN 99], [BAR 91], [GOT 77], [HIL 79], [HIL 93], [HOS 79], [KAR 93]).

Banabic's model is a yield criterion for orthotropic sheet metals under plane stress conditions. It has been developed to take into account the particularity of the aluminium alloys which are BCC materials whereas is FCC one [BAN 00].

The yield stress is expressed as following:

$$\overline{\sigma} = \left[a.(b.\Gamma + c.\Psi)^{2k} + a.(b.\Gamma - c.\Psi)^{2k} + (1-a).(2.c.\Psi)^{2k}\right]^{\frac{1}{2k}} \quad [16]$$

where Γ and Ψ are functions of the stress tensor components defined below:

$$\Gamma = M.\sigma_{11} + N.\sigma_{22} \quad [17]$$

$$\Psi = \sqrt{(P.\sigma_{11} + Q.\sigma_{22})^2 + R.\sigma_{12}^2} \quad [18]$$

The coefficients M, N, P, Q and R are defined as following:

$$M = d + e, N = e + f, P = \frac{d-e}{2}, Q = \frac{e-f}{2}, R = g^2 \quad [19]$$

The above equations show that the shape of the yield locus is defined by eight material parameters: a, b, c, d, e, f, g and k.

The k-parameter can take only two integer values: 3 or 4 depending on the crystallographic structure of the material. For steel and all other FCC materials, $k = 3$. In the contrary for BCC materials as aluminium alloys, $k = 4$. Then only seven material parameters defined the Banabic's yield criterion.

The constitutive law is given for the first component:

$$D_{11} = 2.\dot{\bar{\varepsilon}}.k.\left[\begin{array}{l} a(b.\Gamma + c.\Psi)^{2k-1}(b.M + c.P.\dfrac{P.\sigma_{11} + Q.\sigma_{22}}{\Psi}) + \\ a.(b.\Gamma - c.\Psi)^{2k-1}(b.M - c.P.\dfrac{P.\sigma_{11} + Q.\sigma_{22}}{\Psi}) + \\ 2.c.(1-a).(2.c.\Psi)^{2k-1} P.\dfrac{P.\sigma_{11} + Q.\sigma_{22}}{\Psi} \end{array}\right] \quad [20]$$

The perturbation and the linearization of equation [20] is given in appendix 2.

2.2.2. *Damaged material*

The damage model chosen in this study is an extension of the model proposed by Gelin and Predeleanu [GEL 92]. In that case the plastic flow is governed by the following equation:

$$D_{ij} = \lambda.s_{ij} + \mu.\delta_{ij} \quad [21]$$

with:

$$\lambda = z.\frac{\dot{\bar{\varepsilon}}}{\bar{\sigma}} + A \quad [22]$$

$$\mu = \frac{\bar{\sigma}.\dot{\bar{\varepsilon}}}{\bar{\sigma} + A}.A \quad [23]$$

$$A = \frac{1}{2}.\beta.\ln(\theta^d).trace(\underline{\sigma}).\exp\left[\frac{trace(\underline{\sigma})}{2.\sigma_0(\bar{\varepsilon},\dot{\bar{\varepsilon}})}\right] \quad [24]$$

$$\underline{s} = \underline{\underline{P}} : \underline{\sigma} \quad [25]$$

$$\bar{\sigma} = \underline{\underline{P}} : \underline{\sigma} : \underline{\sigma} \quad [26]$$

The z – parameter can take only two values: $z = \frac{3}{2}$ in case of isotropic material and $z = 1$ in case of orthotropic material described with the Hill 48 plastic criterion. The combination of this damage model with Banabic's yield locus has not been studied yet. $\underline{\underline{P}}$ is a fourth order tensor and is a deviatoric operator. In case of isotropic material, $\underline{\underline{P}} : \underline{\sigma} = dev\underline{\sigma}$ and in case of orthotropic material described with the Hill's fourth order tensor, $\underline{\underline{P}} : \underline{\sigma} = \underline{\underline{H}} : \underline{\sigma}$.

θ^d is the volume change associated with damage evolution and σ_0 is the strain rate-dependent hardening law [1]. θ^d is related to the void volume fraction f by:

$$\theta^d = \frac{1 - f_0}{1 - f} \quad [27]$$

The material is then compressible and the mass conservation condition is expressed as below:

$$trace\ \underline{D} = \frac{\dot{\theta}^d}{\theta^d} \quad [28]$$

The equations obtained by the perturbation of [21] followed by a first order Taylor's development can be found in [BOU 00].

2.2.3. *Post-processing of FE results*

The necking criterion established with the linearized perturbation technique can be easily interfaced to FE programs for necking prediction from FE results. Figure 2 resumes the method.

At each step of a FE calculation the program gives the stress and the strain state corresponding to the current mechanical equilibrium. The calculation of the η-roots can be done very quickly and integration points where necking occurs can be determined very easily without complicated software developments. The necking zones can be revealed by post-processing the FE results.

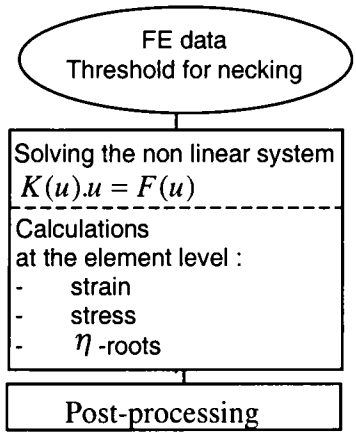

Figure 2. *Implementation of necking criterion based on perturbations technique in a FE program*

3. Simulations and prediction of necking

Two kinds of results will be presented in this section.

In the first subsection local simulations are carried out to improve the different models used. The 3D- and the 2D-stress state approaches are compared. The classical FLD or the $\left(\bar{\varepsilon}^*, \rho\right)$ diagram will be used for the illustrations where $\bar{\varepsilon}^*$ is the effective strain at necking and $\rho = \varepsilon_2 / \varepsilon_1$ is the strain path.

In the second subsection FE simulations of deep-drawing processes are performed and necking predictions are presented and compared to experimental observations.

3.1. *Local simulations*

3.1.1. *3D modelling of necking*

Figure 3 shows the necking strain calculated from 2D or 3D modelling. For the 3D modelling no pressure was imposed meaning that $\sigma_{33} = 0$ along the normal to the sheet metal. For the 2D case, an optimum threshold (different in the thinning domain

than in the expansion one) has been used and for the 3D case an unique threshold has been used.

That explains the difference of shape between the 2D and the 3D FLD in the expansion domain first and secondly the too high level for the 3D FLD in the expansion domain. The strain level is superior in case of 3D modelling for negative strain path. This curve demonstrates that 2D and 3D-modelling are strongly different. The difference is due to the fact that necking is searched not only in plane but also in the thickness of the sheet. The increasing of the strain level at necking in the thinning domain are in agreement with [ITO 00]. The results in the expansion domain are somewhat different compared to results presented in [ITO 00].

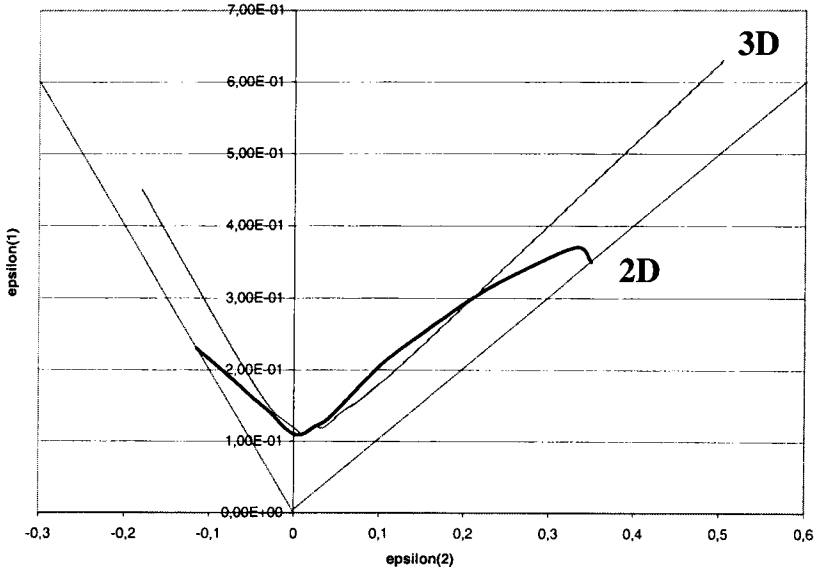

Figure 3. *Comparison between the 2D and the 3D modelling of necking*

3.1.2. *Influence of the yield surface*

Banabic yield criterion allows distinguishing materials with BCC or FCC structure. Necking predictions have been made with the 2D-stress state modelling working with Hill 48 criterion or Banabic criterion.

First the relationship between the strain path and the stress path has been built in Figure 4 for a steel and an aluminium (table 1). Figure 4 shows that the (α, ρ) relationship obtained for a steel (FCC structure) in closer to the linear relationship obtained for Hill 48 than the one obtained for an aluminium (BCC structure).

$\alpha = \sigma_2 / \sigma_1$ is the stress ratio. That proves that the use of Banabic's plastic yield surface will allow necking prediction for larger range of materials.

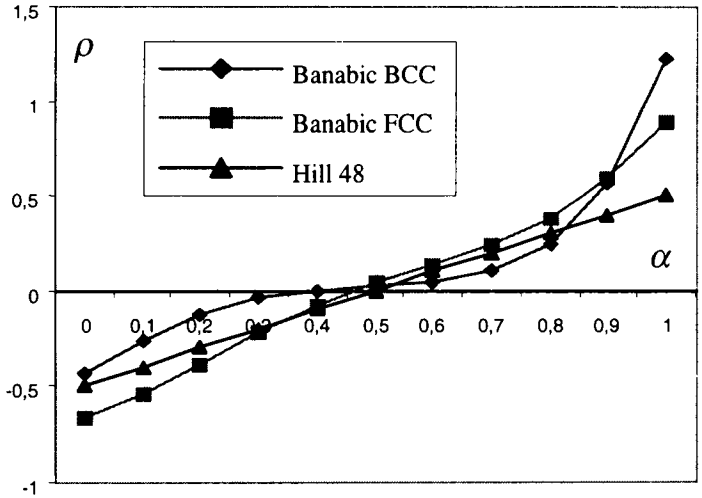

Figure 4. *Illustration of the effect of the plasticity model on the* $\rho = f(\alpha)$ *curves in comparison with the Hill quadratic model (from [LES 00])*

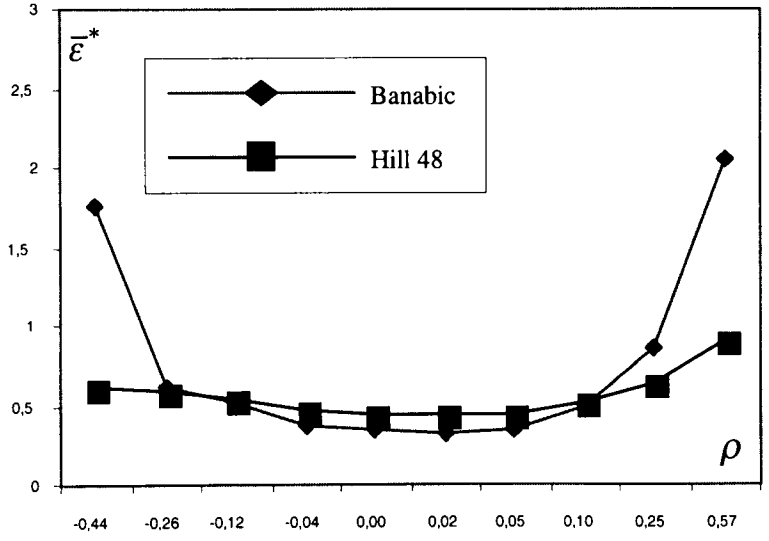

Figure 5. *Comparison of necking predictions using the Hill quadratic plastic criterion and the Banabic's one for an aluminium (from [LES 00])*

Secondly the diagram $(\bar{\varepsilon}^*, \rho)$ has been built for an aluminium with the Hill 48 criterion and with Banabic's criterion (Figure 5). The strain level at necking for the extreme strain paths are very different and it is shown that Hill criterion underestimates the formability. In the contrary strain level at necking for strain path close to plane strain are diminished a little.

This study shows clearly that the yield surface modelling is very important for necking evaluation.

	A	b	C	M	N	p	q	R	k
Aluminium	0.6512	0.9521	0.0987	0.4881	0.5659	5.2209	-5.2598	98.672	4
Steel	0.2115	0.9941	0.8390	0.5811	0.5571	0.5923	-0.5803	1.1548	3

Table 1. *Material parameters for Banabic's yield locus*

3.2. *FE simulations and necking prediction*

The simulations presented in this section have been performed with Stampform®, the FE code developed in our laboratory and dedicated to the simulation of deep-drawing processes. Several hardening laws and yield criteria are available. In the present cases the material is considered isotropic and a Swift hardening law is chosen.

3.2.1. *Stamping of an industrial automotive part*

This part is obtained in two operations and necking is known to appear in the first stage. The part is a 200 x 250 mm^2 sheet metal with 3 mm of thickness. The steel parameters are summarised in table 2.

Necking zones predicted with the perturbations technique are shown in Figure 6 and are in good agreement with experiments. Necking is detected for 28 mm punch displacement as ductile fracture is observed for 29 mm of displacement. The comparison of necking zones with critical thinning zones shows that necking criterion based only on geometrical aspects (critical thinning) are not efficient. For the present example, necking criterion based on the perturbations technique is in good agreement with experiments.

	Automotive part	Cross tool
Young modulus	$E = 206\ 800\ MPa$	$E = 70000 MPa$
Poisson coefficient	$\nu = 0.3$	$\nu = 0.3$
Yield stress	$\sigma_Y = 259 MPa$	$\sigma_Y = 259 MPa$
Hardening law	$K = 562.3 MPa$ $n = 0.241$ $\varepsilon_0 = 0.0256$	$K = 419 MPa$ $n = 0.237$ $\varepsilon_0 = 0.0001$
Damage	$f_0 = 0$ (no damage)	$f_0 = 0$ (no damage)
Anisotropy	$H = 0.6154$ $F = 0.3846$ $P = 1.6153$	Isotropic

Table 2. *Material parameters for deep-drawing simulations*

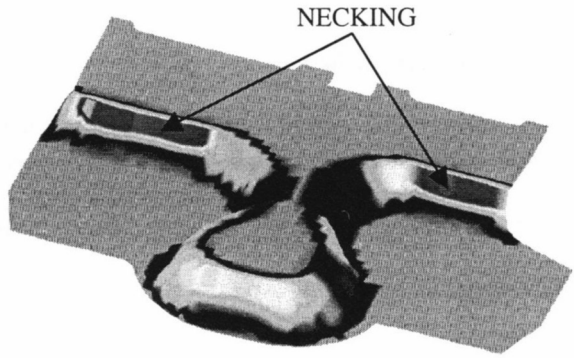

Figure 6. *Necking zones predicted in an industrial automotive part*

3.2.2. *Deep-drawing with a cross-tool*

The geometry of both cross-tool and sheet metal is visible in Figure 7. The aluminium parameters are given in table 2.

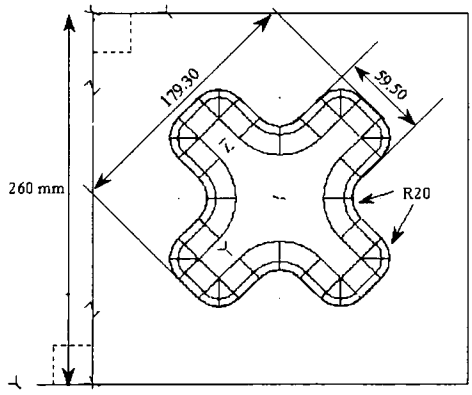

Figure 7. *Geometry of the sheet and of the cross-tool*

Figure 8 shows the necking zones predicted for a 50 mm punch displacement that are in good agreement with experiments.

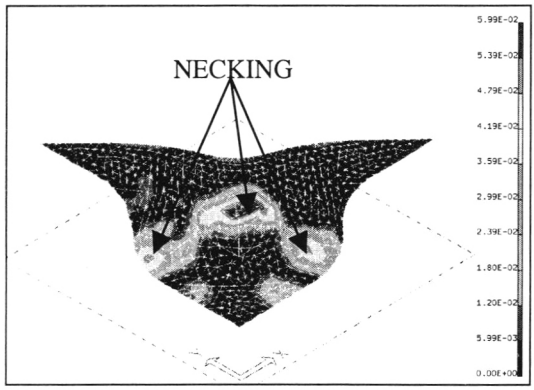

Figure 8. *Necking zones in the cross-tool deep-drawing*

4. Conclusions

This paper reveals several important tendencies concerning necking prediction. First the linear perturbations technique is a very flexible method that covers a very large domain of applications. The technique initially developed for 2D-stress has been extended to 3D-stress states. The adaptation to more accurate plasticity criterion as Banabic's yield locus can be done without problem. As the linear stability analysis analyses the current state, its implementation in a FE code does not need specific and complex developments. All these possibilities have been demonstrated in the paper.

Moreover this approach can be integrated into quality functions to optimise the deep-drawing processes.

An apparent inconvenience of the approach is the complexity of the analytical calculations as it is shown in appendices. But nowadays this is no more a major problem with all the formal calculation software and the numerous interfaces existing between these software and the programming languages.

5. References

[ARR 89] ARRIEUX R., Boivin M., "Theoretical determination of the forming limit stress curve for isotropic sheet materials", *Annals of the CIRP*, 38/1, 1989, p. 261-264.

[BAN 99] BANABIC D., BALAN T., POHLANDT K., "Analytical and experimental investigation on anisotropic yield criteria", *6th Int. Conf. ICTP'99*, Nuremberg, 1999, p. 1411-1416.

[BAN 00] BANABIC D., COMSA D.S., BALAN T., "A new yield criterion for orthotropic sheet metals under plane-stress conditions", *Proc. of TPR 2000*, International section, Cluj-Napoca, 11-12 May, 2000, p. 217-224.

[BAR 91] BARLAT F., LEGE D.J., BREM J.C., "A six-component yield function for anisotropic materials", *Int. J. of Plasticity*, Vol. 7, 1991, p. 693-712.

[BAS 77] BASSANI J.L., "Yield characterisation of metals with transversally isotropic plastic properties", *Int. J. Mech. Sci.*, Vol. 19, 1977, p. 651-654.

[BOU 94] BOUDEAU N., GELIN J.C., "Prediction of the localized necking in 3D sheet metal forming processes from FE simulations", *J. of Mat. Process. Tech.*, V. 45, 1994, p. 229-235.

[BOU 00] BOUDEAU N., GELIN J.C., "Necking in sheet metal forming. Influence of macroscopic and microscopic properties of materials", *Int. J. Mech. Sci.*, Vol. 42, 2000, p. 2209-2232.

[BRU 95] BRUNET M., ARRIEUX R., NGUYEN NHAT T., "Necking prediction using forming limit stress surfaces in 3D sheet metal forming simulation", *Proc. of Numiform'95*, 1995.

[BRU 97] BRUNET M., MGUIL-TOUCHAL S;, MORESTIN F., "Numerical and experimental analysis of necking in 3D sheet metal forming processes using damage variable", in *Advanced Methods in Materials Processing Defects*, edited by M. Predeleanu and P. Gilormini, 1997, p. 205-215.

[FRO 98] FROMENTIN S., Etablissement d'un critère de striction intrinsèque des tôles et validation numérique par simulations d'emboutissage, Ph.D. thesis, University of Metz, France, 1998.

[GEL 92] GELIN J.C., PREDELEANU M., "Recent advances in damage mechanics: modelling and computational aspects", *Fourth International Conference on Numerical Methods in Industrial Forming Processes*, edited by Chenot J.L. *et al.*, 1992, p. 89-98.

[GOO 68] GOODWIN G.M., "Application of the strain analysis to steel metal forming in press shop", *La Metallurgia Italiana*, n° 8, 1968, p. 767-772.

[GOT 77] GOTOH M., "A theory of plastic anisotropy based on a yield function of fourth order", *Int. J. Mech. Sci.*, Vol. 19, 1977, p. 505-520.

[HIL 48] HILL R., "A theory of the yielding and plastic flow of anisotropic metals", *Proc. Roy. Soc.*, London, A 193, 1948, p. 281-297.

[HIL 52] HILL R., "On discontinuous plastic states, with special references to localized necking in thin sheets", *J. Mech. Phys. Solids*, Vol. 1, 1952, p. 19-30.

[HIL 79] HILL R., "Theoretical plasticity of textured aggregates", *Math. Proc. Cambridge Philosophical Soc.*, Vol. 85, 1979, p. 179-191.

[HIL 93] HILL R., "A User-friendly theory of orthotropic plasticity in sheet metals", *Int. J. Mech. Sci.*, Vol. 15, 1993, p. 19-25.

[HOR 96] HORA P., TONG L., REISSNER J., "Prediction method for ductile sheet metals failure in FE simulation", *Third Int. Conf. In Numerical Simulation of 3D Sheet Metal Forming Processes*, edited by J.K. Lee *et al.*, 1996, p. 252-256.

[HOS 79] HOSFORD W.F., "On Yield loci of anisotropic cubic metals", *Proc. 7th North American Metalworking Conf.*, SME, Dearborn, MI, 1979, p. 191-197.

[ITO 00] ITO K., SATOH K., GOYA M., YOSHIDA T., "Prediction of limit strain in sheet metal-forming processes by 3D analysis of localized necking", *Int. J. Mech. Sci.*, Vol 42, n° 11, 2000, p. 2233-2248.

[KAR 93] KARAFILLIS A.P., BOYCE M.C., "A general anisotropic yield criterion using bounds and a tranformation weighting tensor", *J. Mech. Phys. Solids*, Vol. 41, 1993, p. 1859-1886.

[KEE 65] KEELER S.P., "Determination of the forming limits in automotive stamping", *Sheet metal industries*, Vol 42, n° 461, 1965, p. 683-691.

[KNO 00] KNOCKAERT R., MASSONI E., CHASTEL Y., "Prediction of strain localization during sheet forming operations", *Third ESAFORM Conference on Material Forming*, Stuttgart, Deutschland, 2000, II, p. 7-10.

[LES 00] LESTRIEZ P., Prédiction de striction localisée par l'analyse linéarisée de stabilité: application au critère de plasticité de BANABIC, Rapport de DEA, Université de Franche-Comté - ENSMM, France, Septembre 2000.

[MOL 85] MOLINARI A., "Instabilité thermoviscoplastique en cisaillement simple", *Journal de Mécanique Théorique et Appliquée*, Vol 4, n° 5, 1985, p. 659-684.

6. Appendix

6.1. *Appendix 1*

The perturbed equations for the local equilibrium in case of 3D-stress state are:

$$\eta.\sin\varphi.\cos\psi.\delta\sigma_{11} + \eta.\sin\varphi.\sin\psi.\delta\sigma_{12} + \eta.\cos\varphi.\delta\sigma_{13} + \gamma_1.\delta D_{33} = 0$$
$$\eta.\sin\varphi.\sin\psi.\delta\sigma_{22} + \eta.\sin\varphi.\cos\psi.\delta\sigma_{12} + \eta.\cos\varphi.\delta\sigma_{23} + \gamma_2.\delta D_{33} = 0$$
$$\eta.\cos\varphi.\delta\sigma_{33} + \eta.\sin\varphi.\sin\psi.\delta\sigma_{23} + \eta.\sin\varphi.\cos\psi.\delta\sigma_{13} + \gamma_3.\delta D_{33} = 0$$

With: $\gamma_i = \sin\varphi.\cos\psi.\sigma_{i1} + \sin\varphi.\sin\psi.\sigma_{i2} + \cos\varphi.\sigma_{i3}$

The perturbation of the compatibility equations in case of 3D-stress state gives:

$$\sin^2\psi.\delta D_{11} + \cos^2\psi.\delta D_{22} - 2.\cos\psi.\sin\psi.\delta D_{12} = 0$$
$$\cos^2\psi.\delta D_{22} + \sin^2\varphi.\sin^2\psi.\delta D_{33} - 2.\sin\varphi.\cos\varphi.\sin\psi.\delta D_{23} = 0$$
$$\sin^2\varphi.\cos\psi.\sin\psi.\delta D_{33} + \cos^2\varphi.\delta D_{12} - \sin\varphi.\cos\varphi.\cos\psi.\delta D_{23}$$
$$-\sin\varphi.\cos\varphi.\sin\psi.\delta D_{13} = 0$$

6.2. *Appendix 2*

The perturbed equation for the Banabic's yield criterion is the

$$\delta D_{11} = \frac{D_{11}}{\dot{\bar{\varepsilon}}}\delta\dot{\bar{\varepsilon}} + 2.k.\dot{\bar{\varepsilon}}.[\gamma_1.\delta\sigma_{11} + \gamma_2.\delta\sigma_{22} + \gamma_3.\delta\sigma_{12}]$$

$$\gamma_1 = M.\beta_1 + \frac{P.(P.\sigma_{11} + Q.\sigma_{22})}{\Psi}.\beta_2 + \beta_3$$

$$\gamma_2 = N.\beta_1 + \frac{Q.(P.\sigma_{11} + Q.\sigma_{22})}{\Psi}.\beta_2 + \beta_4$$

$$\gamma_3 = \frac{R.\sigma_{12}}{\Psi}.\beta_2$$

$$\beta_1 = \alpha_1.a.(b\Gamma + c\Psi)^{2k-1} + \alpha_3.a.(b\Gamma - c\Psi)^{2k-1} + \alpha_5.(1-a).(2c\Psi)^{2k-1}\frac{2cP}{\Psi}$$

$$\beta_2 = \alpha_2.a.(b\Gamma + c\Psi)^{2k-1} + \alpha_4.a.(b\Gamma - c\Psi)^{2k-1}$$

$$\beta_3 = a.(b\Gamma + c\Psi)^{2k-1}\frac{cP^2}{\Psi} - a.(b\Gamma - c\Psi)^{2k-1}\frac{cP^2}{\Psi} + (1-a).(2c\Psi)^{2k-1}\frac{2cP^2}{\Psi}$$

$$\beta_4 = a.(b\Gamma + c\Psi)^{2k-1}\frac{cPQ}{\Psi} - a.(b\Gamma - c\Psi)^{2k-1}\frac{cPQ}{\Psi} + (1-a).(2c\Psi)^{2k-1}\frac{2cPQ}{\Psi}$$

$$\alpha_1 = \frac{2k-1}{b\Gamma + c\Psi}b\left[bM + \frac{cP}{\Psi}(P\sigma_{11} + Q\sigma_{22})\right]$$

$$\alpha_2 = \frac{2k-1}{b\Gamma + c\Psi}c\left[bM + \frac{cP}{\Psi}(P\sigma_{11} + Q\sigma_{22})\right] - \frac{bM}{\Psi} - \frac{cP}{\Psi^2}(P\sigma_{11} + Q\sigma_{22})$$

$$\alpha_3 = \frac{2k-1}{b\Gamma - c\Psi}b\left[bM - \frac{cP}{\Psi}(P\sigma_{11} + Q\sigma_{22})\right]$$

$$\alpha_4 = -\frac{2k-1}{b\Gamma - c\Psi}c\left[bM - \frac{cP}{\Psi}(P\sigma_{11} + Q\sigma_{22})\right] - \frac{bM}{\Psi} + \frac{cP}{\Psi^2}(P\sigma_{11} + Q\sigma_{22})$$

$$\alpha_5 = \frac{2(k-1)}{\Psi}(P\sigma_{11} + Q\sigma_{22})$$